Computers and Fluids 244 (2022) 105547

Contents lists available at ScienceDirect

Computers and Fluids

journal homepage: www.elsevier.com/locate/compfluid

High order weighted essentially non-oscillatory WENO-ZN schemes for hyperbolic conservation laws

Shiyao Li [a,b], Yiqing Shen [a,b,*], Ke Zhang [a,b], Ming Yu [c]

[a] State Key Laboratory of High Temperature Gas Dynamics, Institute of Mechanics, Chinese Academy of Sciences, Beijing 100190, China
[b] School of Engineering Science, University of Chinese Academy of Sciences, Beijing 100049, China
[c] Center of Applied Physics and Technology, Peking University, Beijing 100871, China

ARTICLE INFO

Keywords:
High-order WENO scheme
Global smoothness indicator
Adaptive function
Critical point

ABSTRACT

In Shen et al. (2020), the authors have proposed a novel weighting method to construct the fifth-order WENO-ZN scheme to improve the accuracy at the second-order critical point. Its basic idea is that, the square of the fourth-order undivided difference on the global five-point stencil used by the fifth-order WENO scheme is suggested as the global smoothness indicator. To keep the ENO property and enhance robustness for resolving shock waves, the constant 1 used to calculate the un-normalized weights in the original WENO-Z schemes is replaced by an adaptive function, which can approach a small value if the global stencil contains a discontinuity or approach a large value if the solution is smooth enough. The fifth-order WENO-ZN scheme can obtain fifth order accuracy at both the first- and second-order critical points. However, limited by the smoothness indicators, the scheme cannot improve the convergence rate at the third-order and above critical points. In this paper, we extend the idea of the fifth-order WENO-ZN scheme to construct higher-order WENO-ZN schemes and investigate their performance. Numerical experiments show that the $(2r-1)$th-order $(r \geq 3)$ WENO-ZN schemes are robust for capturing shock waves and can improve the accuracy order in smooth regions including the maximum $(2r-4)$th-order critical points.

1. Introduction

Numerical simulation is a practical as well as efficient method in the study of shock waves, which is an interesting but complicated phenomenon in fluid dynamics. For its outstanding performance in capturing shock waves and small-scale structures, weighted essentially non-oscillatory (WENO) schemes have been widely studied and applied in computational fluid dynamics.

Harten [1] first proposed essentially non-oscillatory (ENO) scheme with the idea of choosing the smoothest sub-stencil in the reconstruction domain so that the scheme can capture discontinuities and meanwhile achieve high order in smooth regions. Liu et al. [2] developed this idea by using a weighted combination of each candidate sub-stencil instead of choosing the smoothest one and hence the proposed scheme utilized intact information of computing domain and achieve higher order than ENO scheme. Jiang and Shu [3] then exploited higher order variations to calculate smoothness indicators of stencils and introduced a general form of WENO scheme. Since then many efforts have been taken to improve the accuracy and efficiency of the WENO scheme. Henrick et al. [4] pointed out that the WENO scheme implemented by Jiang and Shu (WENO-JS) would lose order at critical points and then derived the necessary and sufficient conditions on the weights of fifth-order WENO schemes to achieve fifth-order convergence. Then they constructed the WENO-M scheme with a mapping function to correct the weights and the scheme satisfies fifth-order convergence condition even at critical points. Borges et al. [5] proposed the WENO-Z scheme with the idea of using the original smoothness indicators to construct a global smoothness indicator (GSI). The global smoothness indicator utilized whole five-points stencil in WENO schemes and helped the WENO-Z scheme achieve similar results to the WENO-M scheme while consuming less computational resources.

The WENO-Z scheme takes nearly the same cost as WENO-JS does but gets better results, which provides an improving direction for WENO schemes. Hu et al. [6] used a six-points global stencil with an extra three-points substencil and a corresponding global smoothness indicator to construct the sixth-order central-upwind WENO-Z type scheme (WENO-CU6). Ha et al. [7] provided a limiter on local smoothness indicator (LSI) and a new sixth-order global smoothness indicator from the five-points stencil. Fan et al. [8] devised new smoothness

* Corresponding author at: State Key Laboratory of High Temperature Gas Dynamics, Institute of Mechanics, Chinese Academy of Sciences, Beijing 100190, China.
E-mail addresses: lishiyao@imech.ac.cn (S. Li), yqshen@imech.ac.cn (Y. Shen), zhangke@imech.ac.cn (K. Zhang), yu_ming@iapcm.ac.cn (M. Yu).

https://doi.org/10.1016/j.compfluid.2022.105547
Received 10 November 2021; Received in revised form 10 May 2022; Accepted 8 June 2022
Available online 14 June 2022

indicators with Lagrangian interpolation polynomial and constructed several new high order global smoothness indicators up to eighth-order. The corresponding WENO-Zη scheme can achieve fifth-order at critical points where the first and second derivatives equal zero. Acker et al. [9] added a new term into the WENO-Z weights to increase the influence of less-smooth substencils and the new scheme (WENO-Z+) attained better resolution in smooth regions. Liu et al. [10] presented a new global smoothness indicator together with a function about the indicator, and the proposed scheme (WENO-ZA) satisfies the sufficient condition for fifth-order convergence even at critical points and meanwhile maintained low dissipation for discontinuous solutions. Recently, Baeza et al. [11] designed a novel global smoothness indicator, which defines the new WENO reconstruction (called OWENO) to attain the optimal order in smooth regions regardless of the presence of critical points of any order. Then the method was extended to develop the third-order OWENO scheme with an additional node [12]. Shen et al. [13] proposed an adaptive function to replace the constant 1 used in nonlinear weight formulations of WENO-Z scheme. The adaptive function can approach a large value when the global stencil is relatively smooth while the global stencil contains a discontinuity then the function approaches a small value. The scheme proposed by Shen et al. (WENO-ZN) can capture shocks robustly and meanwhile reduce dissipation in smooth regions.

In addition to modifying the nonlinear weights of the weighted essentially non-oscillatory schemes, another way to improve the performance of WENO schemes is to increase the convergence order of the nonlinear weights. Balsara and Shu [14] designed a class of higher order WENO schemes up to 11th order of accuracy. Gerolymos et al. [15] further extended WENO schemes to very-high-order. Balsara et al. [16,17] then utilized Legendre polynomials to construct the smoothness indicator, which provided an elegant and compact approach extend WENO schemes to higher order convergence. Shen and Zha [18] developed the seventh-order WENO-Z scheme and discussed the sufficient condition for seventh-order accuracy. Castro et al. [19] devised the optimal higher order global smoothness indicators and investigated the accuracy of the high-order WENO-Z schemes at critical points. Fan [20] extended the WENO-Zη schemes to high odd-orders of accuracy, but the WENO-Zη schemes produce strong oscillations (see the results given in [20]).

In [13], Shen et al. discussed the roles of the global smoothness indicator τ and the constant 1 used for computing the nonlinear weights in WENO-Z schemes. The authors suggested using the square of the fourth-order undivided difference (which is the maximum-order difference) on the global five-point stencil used by the fifth-order WENO scheme as the global smoothness indicator to obtain the high-order approximation of the ideal weights, and constructed an adaptive function of local smoothness indicator to replace the constant 1. If the global stencil contains a discontinuity, the adaptive function will approach a small value, which can capture shocks robustly; and if the global stencil is sufficiently smooth, the adaptive function will approach a large value to improve accuracy and reduce dissipation. The new fifth-order WENO scheme is robust for capturing shocks and can achieve fifth order convergence rate at both the first- and second-order critical points. However, limited by the smoothness indicators, the new scheme cannot improve the convergence rate at the third-order and above critical points.

The high order critical points measure the different scales structures in the complex flow fields [21], for example, the first-, second- and third-order critical points measure the extrema, curvature and inflection, respectively. The numerical simulation of complex compressible flow fields, especially the large eddy simulation (LES) or direct numerical simulation (DNS), requires the used numerical method should have a strong capability for shock-capturing and high accuracy for different scales structures. The fifth-order WENO-ZN scheme provides a general idea. In this article, we extend the fifth-order WENO-ZN scheme to higher-order schemes and investigate their performance.

Table 1
Coefficients $c_{k,r}$.

r	$k=0$	$k=1$	$k=2$	$k=3$	$k=4$
3	1/10	3/5	3/10		
4	1/35	12/35	18/35	4/35	
5	1/126	10/63	10/21	20/63	5/126

This paper is organized as follows: In Section 2, a brief review of the WENO schemes is given. The high-order extensions of the WENO-ZN scheme are presented in Section 3. Section 4 gives several numerical results to validate the performance of high order WENO-ZN schemes. Concluding remarks are given in Section 5.

2. Review of the WENO schemes

Considering the scalar hyperbolic conservation law

$$\frac{\partial u}{\partial t}+\frac{\partial f(u)}{\partial x}=0, \tag{1}$$

where the flux function $f(u)$ can be split into two parts as $f(u)=f^{+}(u)+f^{-}(u)$ with $\mathrm{d}f^{+}(u)/\mathrm{d}u\geqslant 0$ and $\mathrm{d}f^{-}(u)/\mathrm{d}u\leqslant 0$. On a structured grid where $x_i=i\Delta x,(i=0,\ldots,N)$ and Δx is the grid spacing, Eq. (1) can be written in a semi-discrete form as

$$\frac{\mathrm{d}u_i}{\mathrm{d}t}=-\frac{\hat{f}_{i+1/2}-\hat{f}_{i-1/2}}{\Delta x}, \tag{2}$$

in which $\hat{f}_{i\pm1/2}=\hat{f}^{+}_{i\pm1/2}+\hat{f}^{-}_{i\pm1/2}$ is the numerical flux. Without loss of generality, in the following article only the positive part $\hat{f}^{+}_{i\pm1/2}$ will be discussed and the superscript '+' will be dropped for simplicity. The negative part $\hat{f}^{-}_{i\pm1/2}$ can be calculated by the symmetric rule.

In general, the numerical flux of the $(2r-1)$th WENO scheme [14] can be written as

$$\hat{f}_{i+1/2}=\sum_{k=0}^{r-1}\omega_{k,r}q_{k,r}, \tag{3}$$

where $q_{k,r}$ is the rth-order flux on the sub-stencil $S^r_k=(x_{i+k-r+1},x_{i+k-r+2},\ldots,x_{i+k})$ given by

$$q_{k,r}=\sum_{l=0}^{r-1}d_{kl,r}f_{i+k+l-r+1} \tag{4}$$

and $\omega_{k,r}$ is called the weight of the substencil S^r_k. There are several methods to calculate the weights [3–5]. For example, the method proposed by Jiang and Shu [3] is

$$\omega_{k,r}=\frac{\alpha_{k,r}}{\sum_{l=0}^{r-1}\alpha_{l,r}},\quad \alpha_{k,r}=\frac{c_{k,r}}{(\beta_{k,r}+\epsilon)^{p}}, \tag{5}$$

where, ϵ is a small real number used to avoid division by zero, and p is a constant which can control the magnitude of the numerical dissipation. $c_{k,r}$ is the optimal weights given in Table 1.

This paper mainly develops higher order WENO scheme, for completeness and convenience, the related coefficients $d_{kl,r}$ of the fifth-, seventh-, and ninth-order WENO schemes are given in Table 2. One also can refer the Refs. [3,14].

For calculating the weight ω_k Eq. (5), the smoothness indicator $\beta_{k,r}$, which is used to measure the smoothness of the numerical flux on the substencil S^r_k, plays a very important role. In the first WENO scheme proposed by Liu et al. [2], β^r_k is given as

$$\beta^r_k=\sum_{l=1}^{r-1}\sum_{i=1}^{r-l}\frac{(f[j+k+i-r,l])^2}{r-l} \tag{6}$$

where $[\cdot,\cdot]$ is the lth undivided difference operator. To improve accuracy, Jiang and Shu [3] exploited interpolation polynomial to construct the local smoothness indicator as

$$\beta^r_k=\sum_{l=1}^{r-1}\int_{x_{j-1/2}}^{x_{j+1/2}}h^{2l-1}(q^{(l)}_k)^2\mathrm{d}x \tag{7}$$

Table 2
Coefficients d_{kl}^{r}.

r	k	$l=0$	$l=1$	$l=2$	$l=3$	$l=4$
3	0	1/3	−7/6	11/6		
	1	−1/6	5/6	1/3		
	2	1/3	5/6	−1/6		
4	0	−1/4	13/12	−23/12	25/12	
	1	1/12	−5/12	13/12	1/4	
	2	−1/12	7/12	7/12	−1/12	
	3	1/4	13/12	−5/12	1/12	
5	0	1/5	−21/20	137/60	−163/60	137/60
	1	−1/20	17/60	−43/60	77/60	1/5
	2	1/30	−13/60	47/60	9/20	−1/20
	3	−1/20	9/20	47/60	−13/60	1/30
	4	1/5	77/20	−43/60	17/60	−1/20

Table 3
Coefficients $\alpha_{kl,j}$ for $r=4$.

k	l	$j=0$	$j=1$	$j=2$	$j=3$
0	1	−19/60	87/60	−177/60	109/60
	2	−1/2	2	−5/2	1
	3	−1/6	1/2	−1/2	1/6
1	1	11/60	−63/60	33/60	19/60
	2		1/2	−1	1/2
	3	−1/6	1/2	−1/2	1/6
2	1	−19/60	−33/60	63/60	−11/60
	2	1/2	−1	1/2	
	3	−1/6	1/2	−1/2	1/6
3	1	−109/60	177/60	−87/60	19/60
	2	1	−5/2	2	−1/2
	3	−1/6	1/2	−1/2	1/6

where $q_k^{(l)}$ is the lth-derivative of the interpolation polynomial $q_k(x)$. For $r=2$ and 3, the local smoothness indicator defined by Eq. (7) is easily to be evaluated with Taylor expansion. But for $r \geqslant 4$, evaluating the explicit form of β_k^r seems a tedious work [14].

Balsara et al. [16,17] proposed a more compact and elegant method to compute the local smoothness indicator. Using the Hermite polynomials on the domain $[-1/2, 1/2]$

$$H_0(\xi)=1; \quad H_1(\xi)=\xi; \quad H_2(\xi)=\xi^2-\frac{1}{12}; \quad H_3(\xi)=\xi^3-\frac{3}{20}\xi$$
$$H_4(\xi)=\xi^4-\frac{3}{14}\xi^2+\frac{3}{560} \tag{8}$$

the spatially reconstructed polynomials are given by

$$P_i^r(\xi)=p_{i,k}^{[0]}+p_{i,k}^{[1]}H_1(\xi)+\cdots+p_{i,k}^{[r-1]}H_{r-1}(\xi); \quad \xi\in[x_i-\frac{1}{2}\Delta x, x_i+\frac{1}{2}\Delta x] \tag{9}$$

where, $p_{i,k}^{[l]}$ is the difference approximation of the lth derivative $f^{(l)}$ at the substencil S_k^r

$$p_{i,k}^{[l]}=\sum_{j=0}^{r-1}\alpha_{kl,j}f_{i+k+j-r+1}. \tag{10}$$

As an example, Table 3 gives the related coefficients $\alpha_{kl,j}$ of the case $r=4$. Then the local smoothness indicators are calculated as

$$\beta_k=\left(p_k^{[1]}+\frac{p_k^{[3]}}{10}\right)^2+\frac{13}{3}\left(p_k^{[2]}\right)^2+\frac{781}{20}\left(p_k^{[3]}\right)^2; \quad (k=0,1,2,3). \tag{11}$$

The necessary and sufficient conditions on the weights ω_k for the $(2r-1)$th-order WENO scheme to achieve the formal (2r−1) order of convergence rate is given in [4,19] by the truncation error analysis of the finite difference Eq. (2)

$$\begin{cases}\sum_{k=0}^{r-1}A_k(\omega_k^+-\omega_k^-)=O(\Delta x^r)\\ \omega_k^\pm-c_k=O(\Delta x^{r-1}).\end{cases} \tag{12}$$

Table 4
Accuracy of the 7th-order WENO-Z scheme at critical points.

Critical point (Cp)	First term of β_k	First term of τ_7	Order n $(\alpha_k=c_k+O(\Delta x^n))$	
			$q=1$	$q=2$
1st Cp	$A\Delta x^4$	$D\Delta x^6$	2	4
2nd Cp	$B\Delta x^6$	$E\Delta x^8$	2	4
3rd Cp	$C_k\Delta x^8$	$E\Delta x^8$	0	0

*$A=\frac{13}{12}f''^2$, $B=\frac{781}{720}(f^{(3)})^2$, $C_0=C_3=\frac{7373}{2160}(f^{(4)})^2$, $C_1=C_2=\frac{617}{2160}(f^{(4)})^2$ $D=\frac{13}{3}f''f^{(4)}$, $E=\frac{563}{90}(f^{(4)})^2$.

And a sufficient condition for $(2r-1)$th-order convergence is simply given by

$$\omega_k^\pm-c_k=O(\Delta x^r). \tag{13}$$

Henrick et al. [4] constructed the WENO-M scheme with a mapping function to correct the weights of the fifth-order WENO scheme of Jiang and Shu [3]. The WENO-M scheme satisfies fifth-order convergence condition at the first-order critical points. Borges et al. [5] proposed a different method to calculate the weights by introducing a global smoothness indicator, the resulted WENO-Z scheme improves the convergence order at the critical points with a lower computational cost, as well as decreases the dissipation near discontinuities. Later, Castro et al. [19] developed high order WENO-Z schemes.

The general formulations of the normalized and un-normalized weights ω_k^z and α_k^z of the $(2r-1)$th-order WENO-Z scheme are given as [5,19],

$$\omega_{k,r}^z=\frac{\alpha_{k,r}^z}{\sum_{l=0}^{r-1}\alpha_{l,r}^z}, \quad \alpha_{k,r}^z=c_k\left[1+\left(\frac{\tau_{2r-1}}{\beta_k+\varepsilon}\right)^q\right]. \tag{14}$$

The global smoothness indicator τ_{2r-1} is defined as

$$\tau_{2r-1}=\begin{cases}|\beta_0-\beta_{r-1}|, & \mathrm{mod}\ (r,2)=1\\ |\beta_0-\beta_1-\beta_{r-2}+\beta_{r-1}|, & \mathrm{mod}\ (r,2)=0.\end{cases} \tag{15}$$

Wang et al. [21] pointed that the first, second and third order critical point measure the extrema, curvature and inflection, respectively, of the solution and they are usually the most prominent features of flows with large scales structures. The higher order critical points measure the smaller scales structures. It is important for the WENO schemes to resolve the high order critical points as accurate and efficient as possible. There are several papers [5,8,13,19,20,22] analyzed the accuracy order of WENO schemes at critical points.

Clearly, by using the WENO-Z method Eqs. (14)–(15) [5,19], if the first term of τ_{2r-1} is same as that of β_k, then the convergence rate of the WENO-Z scheme will reduce to that of the rth ENO scheme. Here we take the seventh-order WENO-Z scheme as an example to show this issue. For $r=4$, with the Taylor expansions of the local smoothness indicators Eq. (11) at x_i (see Eq. (16) that is given in Box I), there is

$$\tau_7=|\beta_0-\beta_1-\beta_2+\beta_3|=\left|\frac{4}{3}f_i'f_i^{(5)}-\frac{13}{3}f_i''f_i^{(4)}\right|\Delta x^6+O(\Delta x^8). \tag{17}$$

Table 4 gives the accuracy order $n\left(\alpha_k=c_k+O(\Delta x^n)\right)$ of the seventh-order WENO-Z scheme at critical points. q is the power value in Eq. (14). It can be seen that the seventh-order WENO-Z scheme cannot improve the convergence order at third-order critical point, regardless of the power value q.

In [20], Fan constructed another global smoothness indicator that has an optimal order of truncation error of $O(\Delta x^{2r+2})$. The resulted WENO-Zη schemes can improve the accuracy at critical points, but they produce apparent oscillations (see the results given in [20]).

Recently, by a detailed analysis, Baeza et al. [11] designed a novel global smoothness indicator as follows,

$$\tau_D=\frac{d_1^{s1}d_2^{s1}}{d_1^{s1}+d_2^{s1}} \tag{18}$$

$$\begin{cases}\beta_0 = f_i'^2\Delta x^2 + \frac{13}{12}f_i''^2\Delta x^4 - \frac{1}{2}f_i'f_i^{(4)}\Delta x^5 + \left[\frac{781}{720}(f_i^{(3)})^2 + \frac{3}{5}f_i'f_i^{(5)} - \frac{143}{72}f_i''f_i^{(4)}\right]\Delta x^6 + O(\Delta x^7)\\ \beta_1 = f_i'^2\Delta x^2 + \frac{13}{12}f_i''^2\Delta x^4 + \frac{1}{6}f_i'f_i^{(4)}\Delta x^5 + \left[\frac{781}{720}(f_i^{(3)})^2 - \frac{1}{15}f_i'f_i^{(5)} + \frac{13}{72}f_i''f_i^{(4)}\right]\Delta x^6 + O(\Delta x^7)\\ \beta_2 = f_i'^2\Delta x^2 + \frac{13}{12}f_i''^2\Delta x^4 - \frac{1}{6}f_i'f_i^{(4)}\Delta x^5 + \left[\frac{781}{720}(f_i^{(3)})^2 - \frac{1}{15}f_i'f_i^{(5)} + \frac{13}{72}f_i''f_i^{(4)}\right]\Delta x^6 + O(\Delta x^7)\\ \beta_3 = f_i'^2\Delta x^2 + \frac{13}{12}f_i''^2\Delta x^4 + \frac{1}{2}f_i'f_i^{(4)}\Delta x^5 + \left[\frac{781}{720}(f_i^{(3)})^2 + \frac{3}{5}f_i'f_i^{(5)} - \frac{143}{72}f_i''f_i^{(4)}\right]\Delta x^6 + O(\Delta x^7),\end{cases} \tag{16}$$

Box I.

where, d_1 is the squared undivided difference of the $2r-1$ consecutive values $\{f_{i-r+1},\dots,f_{i+r-1}\}$,

$$d_1 = [D^{(2r-2)}(f_{i-r+1},\dots,f_{i+r-1})]^2 \tag{19}$$

and d_2 is defined as

$$d_2 = B^2 - 4AC \tag{20}$$

where A, B and C are the coefficients of the parabola

$$P^{(2r-4)}(w) = C + Bw + Aw^2. \tag{21}$$

$P^{(2r-4)}(w)$ is the $(2r-4)$th derivative of the $(2r-2)$th-degree polynomial $P(w) = p(x_i + w\Delta x)$, where p is the reconstruction polynomial associated with the data $f_{i-r+1},\dots,f_{i+r-1}$. For the fifth-order WENO scheme ($r = 3$), these coefficients can be obtained as

$$\begin{aligned}A &= \frac{1}{2}f_{i-2} - 2f_{i-1} + 3f_i - 2f_{i+1} + \frac{1}{2}f_{i+2},\\ B &= -\frac{1}{2}f_{i-2} + f_{i-1} - f_{i+1} + \frac{1}{2}f_{i+2},\\ C &= -\frac{1}{12}f_{i-2} + \frac{4}{3}f_{i-1} - \frac{5}{2}f_i + \frac{4}{3}f_{i+1} - \frac{1}{12}f_{i+2}.\end{aligned} \tag{22}$$

The weights ω_k is calculated by

$$\omega_k = \frac{\alpha_k^o}{\sum_k \alpha_k^o}, \quad \alpha_k^o = c_k\left[1 + \frac{\tau_D}{\beta_k^{s1} + \epsilon}\right]^{s2}, \quad (k = 0, 1, 2) \tag{23}$$

in which $s1 = 2$ and $s2 = 1$ are suggested and used in [11]. Numerical results show that the new scheme can attain the optimal order regardless of the order of critical points.

Baeza et al. [11] pointed out that the new method does not always outperform existing ones, as it claimed in [5] that improvements in the numerical solution of problems with shocks mainly depend on how far from zero are the weights associated with stencils crossed by discontinuities rather than on the superior accuracy at critical points (especially if they are high-order critical points). They also mentioned that some questions of the OWENO scheme are still open, for example, the influence of the exponents $s1$ and $s2$ in the numerical dissipation and the determination of their optimal values to reduce numerical dissipation as much as possible without generating artifacts or spurious oscillations.

3. The new scheme

3.1. The fifth-order WENO-ZN scheme

In [13], Shen et al. proposed a new method for constructing a fifth-order weighted essentially non-oscillatory scheme to improve the accuracy at the second-order critical point. The basic idea is that, the square of the fourth-order undivided difference at the global five-points stencil is suggested as the global smoothness indicator (τ_8), and an adaptive function θ of the local smoothness indicators is used to replace the constant 1 in Eq. (14) to enhance stability and reduce dissipation. The new scheme is called the fifth-order WENO-ZN scheme. For completeness, we give the formulations as follows,

$$\tau_8 = \left[D^{(4)}f_i\right]^2 = (f_{i-2} - 4f_{i-1} + 6f_i - 4f_{i+1} + f_{i+2})^2, \tag{24}$$

$$\theta = C \times \left(\frac{\beta_0 + \beta_2 - |\beta_0 - \beta_2| + \varepsilon}{|\beta_0 - \beta_2| + \varepsilon}\right)^2, \tag{25}$$

where, C is an constant number. Shen et al. [13] discussed the role of C in the fifth-order WENO-ZN scheme in detail. They showed that $C = 10$ can efficiently increase the contribution of less-smooth substencils in a reasonable region, and hence the numerical resolution of a high frequency wave in relatively coarse grids can be improved.

The un-normalized weight α_k^{ZN} of the fifth-order WENO-ZN scheme is then calculated by

$$\alpha_k^{ZN} = c_k\left[\theta + \left(\frac{\tau_8}{\beta_k + \varepsilon}\right)^q\right]. \tag{26}$$

Numerical results showed that, with $q = 2$, the fifth-order WENO-ZN scheme can achieve fifth-order convergence rate at both the first- and second-order critical points; with $q = 1$ it can achieve fifth-order and fourth-order accuracy at the first- and second-order critical points, respectively. However, as analyzed previously, the fifth-order WENO-ZN scheme cannot help to improve the accuracy order at third-order critical points.

3.2. High order WENO-ZN scheme

In order to meet the demand of resolving the high order critical points with high order accuracy, we extend the fifth-order WENO-ZN scheme to the general scheme of higher order. The un-normalized weights α_k of the $(2r-1)$th order WENO-ZN schemes can be calculated by

$$\alpha_k^{ZN} = c_k\left[\theta + \left(\frac{\tau_{4r-4}}{\beta_k + \varepsilon}\right)^q\right], \tag{27}$$

where q is a tunable parameter. For fifth-order WENO schemes, $q = 1$ is widely used for the sake of less dissipation [5]. For higher order WENO schemes, $q = 2$ is suggested for robustness [19]. The adaptive function θ is given by

$$\theta = C \times \left(\frac{\beta_0 + \beta_{r-1} - |\beta_0 - \beta_{r-1}| + \varepsilon}{|\beta_0 - \beta_{r-1}| + \varepsilon}\right)^2 \tag{28}$$

and the global smoothness indicator τ_{4r-4} is defined as

$$\tau_{4r-4} = \left[D^{(2r-2)}f_i\right]^2, \tag{29}$$

where $D^{(2r-2)}f_i$ is the $(2r-2)$th undivided difference on the global stencil. For example, for $r = 3, 4, 5$, there are

$$\tau_8 = (f_{i-2} - 4f_{i-1} + 6f_i - 4f_{i+1} + f_{i+2})^2, \tag{30}$$

$$\tau_{12} = (f_{i-3} - 6f_{i-2} + 15f_{i-1} - 20f_i + 15f_{i+1} - 6f_{i+2} + f_{i+3})^2, \tag{31}$$

$$\begin{aligned}\tau_{16} = (&f_{i-4} - 8f_{i-3} + 28f_{i-2} - 56f_{i-1} + 70f_i - 56f_{i+1}\\ &+28f_{i+2} - 8f_{i+3} + f_{i+4})^2.\end{aligned} \tag{32}$$

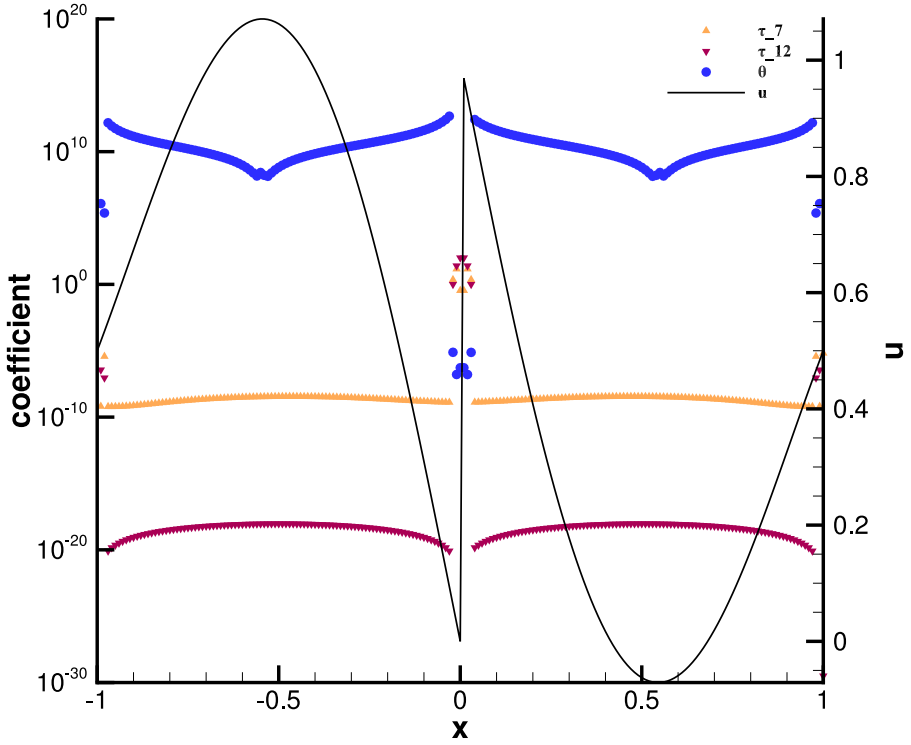

Fig. 1. relative magnitudes of τ_7, τ_{12} and θ.

Table 5
Accuracy of the WENO-ZN schemes at critical points.

	Critical point (Cp)	First term of β_k	First term of τ_{4r-4}	Order $n\left(\alpha_k = c_k + O(\Delta x^n)\right)$	
				$q=1$	$q=2$
$r=3$	1st Cp	$A\Delta x^4$	$\sigma\Delta x^8$	4	8
5th-WENO-ZN	2nd Cp	$B_k\Delta x^6$	$\sigma\Delta x^8$	2	4
	3rd Cp	$C_k\Delta x^8$	$\sigma\Delta x^8$	0	0
$r=4$	1st Cp	$A\Delta x^4$	$\phi\Delta x^{12}$	8	16
7th-WENO-ZN	2nd Cp	$B\Delta x^6$	$\phi\Delta x^{12}$	6	12
	3rd Cp	$C_k\Delta x^8$	$\phi\Delta x^{12}$	4	8
	4th Cp	$D_k\Delta x^{10}$	$\phi\Delta x^{12}$	2	4
	5th Cp	$E_k\Delta x^{12}$	$\phi\Delta x^{12}$	0	0
$r=5$	1st Cp	$A\Delta x^4$	$\psi\Delta x^{16}$	12	24
9th-WENO-ZN	2nd Cp	$B\Delta x^6$	$\psi\Delta x^{16}$	10	20
	3rd Cp	$C\Delta x^8$	$\psi\Delta x^{16}$	8	16
	4th Cp	$D_k\Delta x^{10}$	$\psi\Delta x^{16}$	6	12
	5th Cp	$E_k\Delta x^{12}$	$\psi\Delta x^{16}$	4	8
	6th Cp	$F_k\Delta x^{14}$	$\psi\Delta x^{16}$	2	4
	7th Cp	$G_k\Delta x^{16}$	$\psi\Delta x^{16}$	0	0

*$\sigma = \left(f^{(4)}\right)^2$, $\varphi = \left(f^{(6)}\right)^2$, $\psi = \left(f^{(8)}\right)^2$. Coefficients in first term of β_k can be calculated by using the formula Eq. (11). Note that A, B, and C are independent of k.

3.3. The properties of the WENO-ZN scheme

(1) The accuracy order of the WENO-ZN schemes at critical points can be drawn in Table 5. The high-order WENO-ZN schemes ($r \geq 4$) are more efficient for improving the accuracy at critical points than the high-order WENO-Zη schemes [20], since the order of the global smoothness indicator of WENO-ZN is $O(\Delta x^{4r-4})$ and that of WENO-Zη with the optimal-order global smoothness indicator is $O(\Delta x^{2r+2})$. That is, the $(2r-1)$th-order WENO-ZN scheme can improve the convergence rate at the $(2r-4)$th order critical point, while the $(2r-1)$th-order WENO-Zη scheme can only improve the convergence rate at the critical point with the maximum $(r-1)$th-order.

(2) It is clear that the sub-stencils S_0 and S_{r-1} can completely cover the global stencil, which is used by a WENO scheme, without overlapping. If the global stencil contains a discontinuity, the discontinuity must fall into sub-stencil either S_0 or S_{r-1}. Without loss of generality, assume that the sub-stencil S_0 contains the discontinuity and S_{r-1} is smooth, then there is $\beta_0 \gg \beta_{r-1}$ and hence $\theta \ll 1$. The relative magnitudes of the un-normalized weights α_k^{ZN} are mainly determined by the second term in Eq. (27). Since τ_{4r-4} is independent of k, the ENO property can be kept well by the local smoothness indicator β_k. Otherwise, for a smooth global stencil, from the Taylor series expansions, β_0 and β_{r-1} always have the same leading terms and hence there is $\theta \gg 1$. The large value of θ makes the WENO-ZN schemes have the properties of low dissipation and high resolution.

We take the function $u_0(x)$ Eq. (33) as an example to show the performance of τ_{4r-4}.

$$u_0(x) = \begin{cases} -\sin(\pi x) - \frac{1}{2}x^3, & -1 \leqslant x < 0 \\ -\sin(\pi x) - \frac{1}{2}x^3 + 1, & 0 \leqslant x < 1. \end{cases} \tag{33}$$

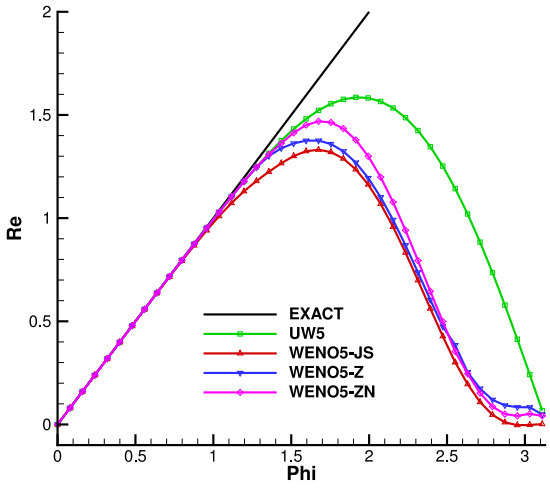

(a) Dispersion of 5th-order schemes

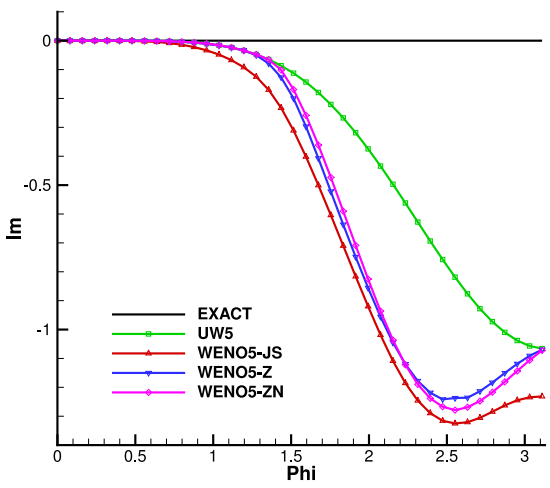

(b) Dissipation of 5th-order schemes

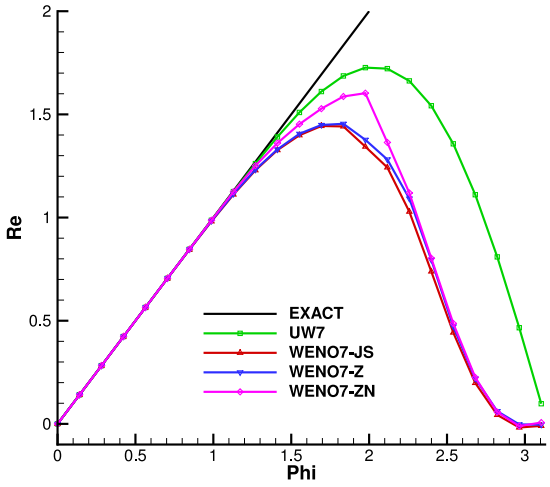

(c) Dispersion of 7th-order schemes

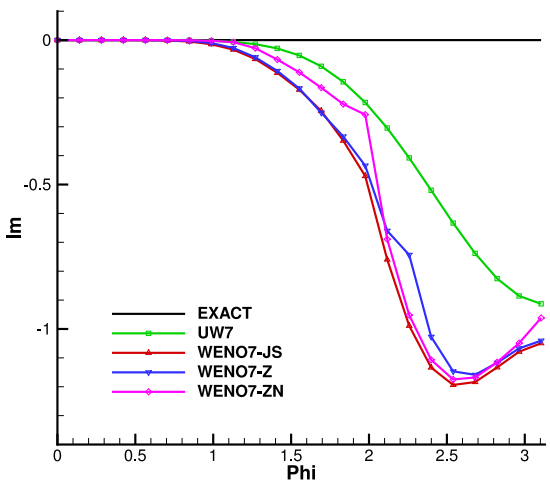

(d) Dissipation of 7th-order schemes

Fig. 2. Spectral properties of schemes.

Fig. 1 gives the curves of τ_7, τ_{12} and θ. It can be seen that, in smooth regions, there are $\theta \gg 1$ and $\tau_7 \gg \tau_{12}$. When the global stencil contains a discontinuity ($x = 0$), there is $\tau_{12} \sim \tau_7 \gg \theta$, so the ENO property is kept and the scheme can capture discontinuity well.

(3) The spectral properties of a nonlinear schemes can be analyzed by the approximate dispersion relation method proposed by Pirozzoli [23]. Fig. 2 gives the comparisons of spectral properties of the WENO-ZN schemes, the WENO-JS schemes, the WENO-Z schemes, and the fifth- and seventh-order linear upstream schemes (UW5 and UW7, respectively). The new schemes maintain low dissipation and dispersion error in a large region of medium wave number.

4. Numerical examples

In this section, the performance of the new schemes are tested by several problems of the linear advection equation, the one-, two- and three-dimensional Euler equations. For readability and brevity, this paper mainly gives and compares the seventh-order schemes. For the ninth-order schemes, we can obtain similar conclusions. The third-order TVD Runge–Kutta method [24] is used for the time integration.

4.1. The accuracy at critical point

The function $f(x) = x^k e^x$ is used to test the convergence rate of WENO schemes at critical point [8]. For this function, the point $x = 0$

Table 6
Convergence order of the 5th-WENO schemes at critical points.

Case	Δx	WENO5-JS		WENO5-Z		WENO5-ZN	
		Error	Order	Error	Order	Error	Order
$k=2$	1.25E−02	2.10E−06	–	1.94E−08	–	1.51E−10	–
1st Cp	6.25E−03	2.36E−07	3.15	4.68E−10	5.37	4.75E−12	4.99
	3.13E−03	2.79E−08	3.08	1.24E−11	5.24	1.49E−13	5.00
	1.56E−03	3.39E−09	3.04	3.53E−13	5.14	4.65E−15	5.00
$k=3$	1.25E−02	1.56E−04	–	1.51E−04	–	4.38E−05	–
2nd Cp	6.25E−03	3.90E−05	2.00	3.51E−05	2.11	1.55E−06	4.82
	3.13E−03	9.75E−06	2.00	7.31E−06	2.26	2.71E−08	5.84
	1.56E−03	2.44E−06	2.00	1.46E−06	2.32	4.33E−10	5.97
$k=4$	1.25E−02	3.18E−08	–	1.31E−08	–	6.89E−08	–
3rd Cp	6.25E−03	2.41E−09	3.72	5.32E−09	1.30	2.64E−08	1.38
	3.13E−03	2.04E−10	3.56	2.38E−09	1.16	5.08E−09	2.38
	1.56E−03	1.94E−11	3.39	5.51E−10	2.11	7.21E−10	2.81

Table 7
Convergence order of the 7th-WENO schemes at critical points.

Case	Δx	WENO7-JS		WENO7-Z		WENO7-ZN	
		Error	Order	Error	Order	Error	Order
$k=3$	1.25E−02	3.43E−09	–	4.51E−11	–	5.67E−14	–
2nd Cp	6.25E−03	4.68E−10	2.87	1.09E−12	5.38	4.45E−16	6.99
	3.13E−03	3.65E−11	3.68	1.95E−14	5.80	3.49E−18	7.00
	1.56E−03	2.50E−12	3.87	3.22E−16	5.92	2.73E−20	7.00
$k=4$	1.25E−02	5.17E−07	–	4.99E−07	–	2.83E−13	–
3rd Cp	6.25E−03	4.42E−08	3.55	4.27E−08	3.55	2.22E−15	6.99
	3.13E−03	4.22E−09	3.39	4.08E−09	3.39	1.74E−17	7.00
	1.56E−03	4.46E−10	3.24	4.31E−10	3.24	1.36E−19	7.00
$k=5$	1.25E−02	9.58E−08	–	9.58E−08	–	6.42E−09	–
4th Cp	6.25E−03	6.02E−09	3.99	6.02E−09	3.99	3.72E−11	7.43
	3.13E−03	3.77E−10	4.00	3.77E−10	4.00	1.68E−13	7.80
	1.56E−03	2.36E−11	4.00	2.36E−11	4.00	6.99E−16	7.91

is the $(k-1)$th-order critical point. The numerical results given in Tables 6–8 show that the accuracy order is in agreement with the theoretical analysis of Tables 4 and 5. WENO5-ZN can obtain at least a fifth-order convergence rate at both the first- and second-order critical points, but it cannot improve the accuracy at the third-order one. While WENO7-ZN can obtain seventh order at the second-, third- and even fourth-order critical points. Similar conclusion can be drawn for the ninth-order WENO-ZN schemes.

It should be pointed out that, there were two kinds of high-order methods proposed to improve the accuracy at critical points. One method is the WENO-Zη schemes proposed by Fan [20], however, the high-order WENO-Zη schemes produce apparent oscillations. The another method, which can be denoted as WENO-ZMq$n$dx$m$ (for example, WENO-Z7q2dx3 denotes the seventh-order WENO-Z scheme $M=7$ with $q=2$ and $\varepsilon=\Delta x^3$), is proposed by Don et al. [22]. Don et al. gave a sufficient condition for achieving the optimal order $(2r-1)$ for a $(2r-1)$th-order WENO-Z scheme Eq. (14), i.e. $\theta(\varepsilon)\le\theta(\tau_{2r-1})-(r-1)/q$, where $\theta(g(\Delta x))$ denotes the power of Δx in the leading term of the Taylor series expansion of $g(\Delta x)$. However, since the spatial step cannot be a nondimensional infinitesimal in practical computing and also the dimensions of β_k and Δx (the operation $\beta_k+\Delta x^m$ is used to calculate the weights α_k, Eq. (14))are different, this kind of WENO-ZMq$n$dx$m$ schemes may generate oscillatory solutions or dissimilar solutions if different reference values are used to nondimensionalize the unknown variable (or computational region). Interested readers can refer [13].

Since the WENO-Zη schemes and the WENO-ZMq$n$dx$m$ schemes cannot keep the ENO property well, in this paper, the two kinds of schemes are not compared and discussed, though they may obtain high-order accuracy at high-order critical points.

Table 8
Convergence order of the 9th-WENO schemes at critical points.

Case	Δx	WENO9-JS		WENO9-Z		WENO9-ZN	
		Error	Order	Error	Order	Error	Order
$k=4$	1.25E−02	3.79E−10	–	5.54E−11	–	2.95E−17	–
3rd Cp	6.25E−03	4.81E−12	6.30	2.30E−13	7.91	5.80E−20	8.99
	3.13E−03	4.35E−14	6.79	7.93E−16	8.18	1.13E−22	9.00
	1.56E−03	3.13E−16	7.12	2.04E−18	8.60	2.22E−25	9.00
$k=5$	1.25E−02	9.63E−08	–	2.16E−08	–	1.77E−16	–
4th Cp	6.25E−03	6.02E−09	4.00	1.61E−09	3.74	3.47E−19	8.99
	3.13E−03	3.76E−10	4.00	1.87E−10	3.11	6.80E−22	9.00
	1.56E−03	2.35E−11	4.00	1.31E−11	3.84	1.33E−24	9.00
$k=6$	1.25E−02	1.31E−10	–	4.98E−08	–	8.86E−16	–
5th Cp	6.25E−03	2.80E−12	5.54	1.67E−09	4.90	1.74E−18	9.00
	3.13E−03	6.75E−14	5.37	5.43E−11	4.95	3.40E−21	9.00
	1.56E−03	1.80E−15	5.23	1.73E−12	4.97	6.65E−24	9.00
$k=7$	1.25E−02	7.63E−11	–	7.90E−09	–	3.66E−11	–
6th Cp	6.25E−03	1.19E−12	6.00	1.34E−10	5.88	2.79E−13	7.04
	3.13E−03	1.86E−14	6.00	2.27E−12	5.89	2.07E−15	7.07
	1.56E−03	2.91E−16	6.00	3.83E−14	5.89	3.79E−18	9.09

4.2. Linear advection problem

The linear advection equation is given by

$$\begin{cases} u_t+u_x=0, & -1\leqslant x\leqslant 1,\\ u(x,0)=u_0(x), & \text{periodic boundary.}\end{cases} \tag{34}$$

with the exact solution at time t

$$u(x,t)=u_0(x-t). \tag{35}$$

The initial condition is

$$u_0(x)=\begin{cases} \frac{1}{6}(G(x,\beta,z-\delta)+G(x,\beta,z+\delta)+4G(x,\beta,z)), & -0.8\leqslant x\leqslant -0.6\\ 1, & -0.4\leqslant x\leqslant -0.2\\ 1-|10(x-0.1)|, & 0\leqslant x\leqslant 0.2\\ \frac{1}{6}(F(x,\alpha,a-\delta)+F(x,\alpha,a+\delta)+4F(x,\alpha,a)), & 0.4\leqslant x\leqslant 0.6\\ 0, & \text{otherwise,}\end{cases} \tag{36}$$

where, same as [3], the functions and constants for this case are taken as

$$G(x,\beta,z)=e^{-\beta(x-z)^2},\ F(x,\alpha,a)=\sqrt{\max(1-\alpha^2(x-\alpha)^2,0)},$$
$$a=0.5,\ z=-0.7,\ \delta=0.005,\ \alpha=10,\ \beta=\log 2/36\delta^2.$$

The solution contains a smooth combination of Gaussian wave, a square wave, a sharp triangle wave and a half ellipse wave. Numerical results of different 7th-order WENO schemes at $t=10$ with a grid of $N=200$ are given in Fig. 3. It can be observed that the WENO-ZN scheme gets the best result, especially for the square wave and the half ellipse wave. The WENO-Z scheme generates an apparent asymmetric solution near the square wave.

4.3. One dimensional Euler problems

The one dimensional Euler equations are given by

$$\frac{\partial U}{\partial t}+\frac{\partial F(U)}{\partial x}=0, \tag{37}$$

where $U=(\rho,\rho u,E)^T$, $F(U)=(\rho u,\rho u^2+p,u(E+p))^T$. Here ρ, u, E, p are density, velocity, total energy and pressure, respectively. For ideal gas $E=\frac{p}{\gamma-1}+\frac{1}{2}\rho u^2$, where $\gamma=1.4$ is the ratio of specific heat. Time step is calculated as

$$\Delta t=\frac{\mathrm{CFL}\Delta x}{\max_i(|u_i|+c_i)}, \tag{38}$$

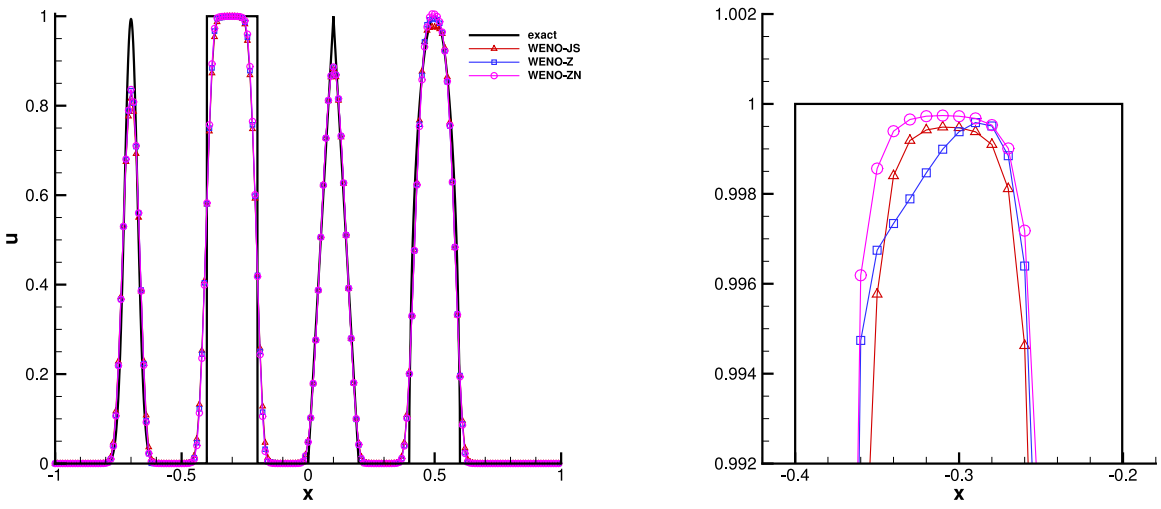

(a) The union wave (b) Zoom in view

Fig. 3. Numerical results of linear advection equation by the 7th-order WENO schemes with $N = 200$ at $t = 10$.

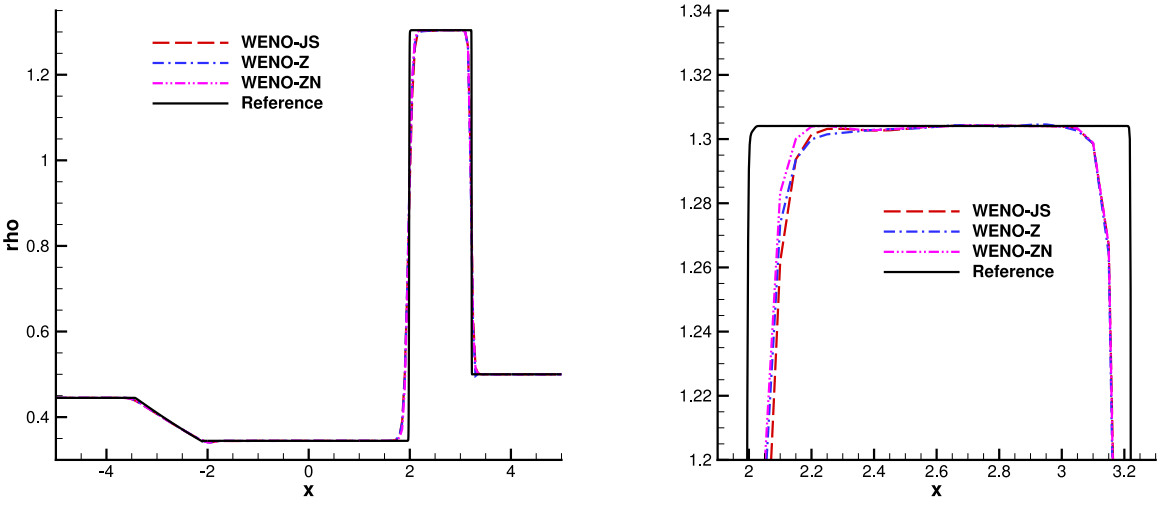

(a) Density distribution (b) Zoom-in view

Fig. 4. Numerical results of the Lax problem computed by the 7th-order WENO schemes with $N = 200$ at $t = 1.3$.

where CFL = 0.5, and $c = \sqrt{\gamma p/\rho}$ is the speed of sound. The global Lax–Friedrichs flux-splitting method and local characteristic fields is used to carry out the 7th-order WENO reconstruction [25].

4.3.1. Riemann initial value problem of lax

The first problem is the Riemann initial value problem of Lax [3], and the initial conditions are given by:

$$(\rho, u, p) = \begin{cases} (0.445,\ 0.698,\ 3.528), & -5 \leqslant x < 0 \\ (0.5,\ 0,\ 0.571), & 0 \leqslant x \leqslant 5. \end{cases} \tag{39}$$

Zero gradient boundary conditions are placed at $x = \pm 5.0$. Fig. 4 gives the distributions of density computed by the seventh-order WENO schemes ($r = 4$) at $t = 1.3$ with $N = 200$. The reference solution is obtained by using $N = 4000$ with the fifth-order WENO-Z scheme. As the figure shows, the WENO-ZN scheme can reduce the numerical dissipation near shock waves.

4.3.2. Shu-Osher problem

The second problem is the Shu–Osher problem [24], which describes the interaction of a Mach 3 shock with a density wave. The initial conditions are given by:

$$(\rho, u, p) = \begin{cases} (\frac{27}{7},\ \frac{4\sqrt{35}}{9},\ \frac{31}{3}), & -5 \leqslant x < -4 \\ (1 + 0.2\sin(5x),\ 0,\ 1), & -4 \leqslant x \leqslant 5 \end{cases} \tag{40}$$

Zero gradient boundary conditions are set at $x = \pm 5.0$. The numerical results from different 7th-order WENO schemes at $t = 1.8$ with $N = 200$ are presented in Fig. 5. The reference solution is obtained by the seventh-order WENO-Z scheme with a grid of 4000. Results show that the WENO-ZN scheme gives better resolved short waves than the WENO-JS and WENO-Z schemes.

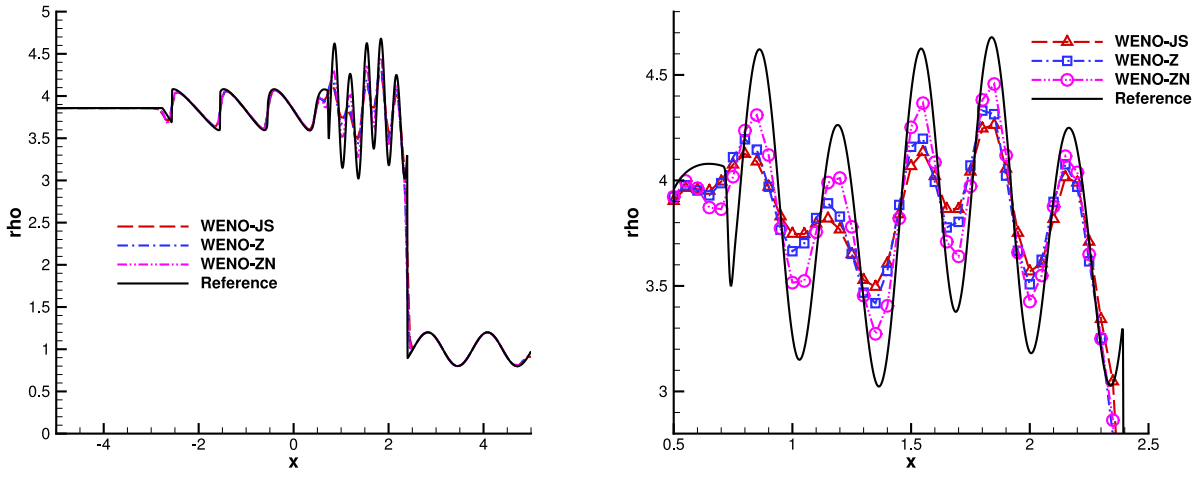

(a) Density distribution (b) Zoom-in view

Fig. 5. Numerical results of the Shu–Osher problem computed by the 7th-order WENO schemes with $N = 200$ at $t = 1.8$.

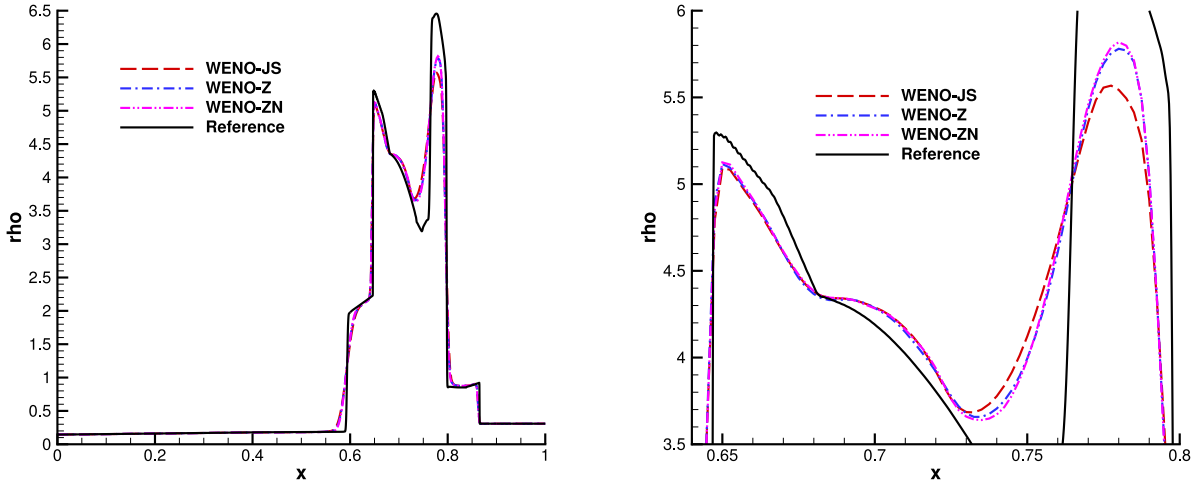

(a) Density distribution (b) Zoom-in view

Fig. 6. Numerical results of the two interacting blast waves problem computed by the 7th-order WENO schemes with $N = 400$ at $t = 0.038$.

4.3.3. *Interactive blast waves problem*

The third problem is the interactive blast waves problem [5] with the initial condition

$$(\rho, u, p) = \begin{cases} (1,\ 0,\ 1000), & 0 \leqslant x < 0.1 \\ (1,\ 0,\ 0.001), & 0.1 \leqslant x < 0.9 \\ (1,\ 0,\ 100), & 0.9 \leqslant x \leqslant 1. \end{cases} \tag{41}$$

Reflective boundary conditions are set at boundaries. Fig. 6 gives the numerical results from 7th-order WENO schemes at $t = 0.038$ with $N = 400$. The reference solution are obtained by the seventh-order WENO-Z scheme with a gird of 4000. It can be seen that three schemes can capture the strong shock wave well. The WENO-ZN scheme is less dissipation than the WENO-JS scheme and the WENO-Z scheme.

4.4. *Two dimensional Euler problems*

The governing equation of two-dimensional Euler problems is given by

$$\frac{\partial U}{\partial t} + \frac{\partial F(U)}{\partial x} + \frac{\partial G(U)}{\partial y} = 0, \tag{42}$$

where

$$U = (\rho, \rho u, \rho v, E)^T,$$
$$F(U) = (\rho u, \rho u^2 + p, \rho uv, (E + p)u)^T,$$
$$G(U) = (\rho v, \rho uv, \rho v^2 + p, (E + p)v)^T.$$

The specific total energy E can be calculated as

$$E = \frac{p}{\gamma - 1} + \frac{1}{2}\rho(u^2 + v^2). \tag{43}$$

The time step is taken as

$$\Delta t = \mathrm{CFL}\frac{\Delta t_x \Delta t_y}{\Delta t_x + \Delta t_y},$$
$$\Delta t_x = \frac{\Delta x}{\max_{i,j}(|u_{i,j}| + c_{i,j})}, \tag{44}$$
$$\Delta t_y = \frac{\Delta y}{\max_{i,j}(|v_{i,j}| + c_{i,j})}.$$

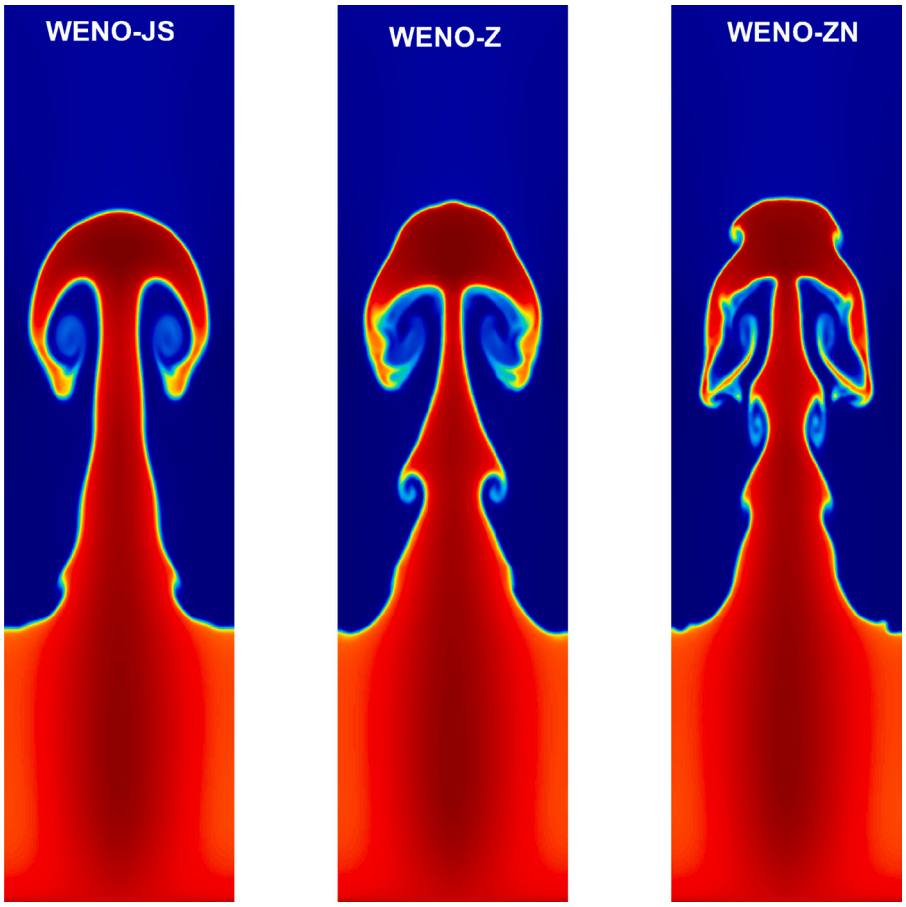

Fig. 7. Density contours for Rayleigh–Taylor instabilities by different 7th-order WENO schemes at $t = 1.95$, $N_x \times N_y = 120 \times 480$.

4.4.1. Rayleigh–Taylor instability

The two-dimensional Rayleigh–Taylor instability problem [26,27] describes the interface instability between fluids with different densities when acceleration is directed from the heavy fluid to the light one. The acceleration effect is introduced by adding ρ and ρv to the flux of the y-momentum and the energy equations, respectively. The problem is often used to test the dissipation property of a high-order scheme. The initial distribution is given by

$$(\rho, u, v, p) = \begin{cases} (2,\ 0,\ -0.025a\cos(8\pi x), 2y+1), & 0 \leqslant y < 0.5 \\ (1,\ 0,\ -0.025a\cos(8\pi x), y+1.5), & 0.5 \leqslant y \leqslant 1, \end{cases} \tag{45}$$

where $a = \sqrt{(\gamma p)/\rho}$ is the speed of sound with $\gamma = 5/3$. The computational domain is $[0, 0.25] \times [0.1]$. The left and right boundaries are reflective boundary conditions, while the top and bottom boundaries are set as $(\rho, u, v, p) = (1, 0, 0, 2.5)$ and $(\rho, u, v, p) = (2, 0, 0, 1)$, respectively. The solution at $t = 1.95$ is solved by different 7th-order WENO schemes with the meshes of 120×480. The density contours are plotted in Fig. 7. Since the inviscid Euler equations are solved, the details of the complex instable structures are related to the numerical dissipation of the used scheme [28]. Due to less dissipation, the WENO-ZN scheme generates richer unstable structures than the other two schemes.

4.4.2. Two-dimensional shock vortex interaction problem

The two-dimensional shock vortex interaction problem taken from [3] is solved to test the dissipation of different schemes. The problem describes the interaction between a stationary shock and a vortex. The computational domain is taken as $[0, 2] \times [0, 1]$. A stationary Mach 1.1 shock is positioned at $x = 0.5$ and normal to the x-axis. Its left state is $(\rho, u, v, p) = (1, 1.1\sqrt{\gamma}, 0, 1)$. A small vortex is superimposed to the flow on the left of the shock and is centered at $(x_c, y_c) = (0.25, 0.5)$. The vortex is described as a perturbation to the velocity (u, v), temperature $(T = p/\rho)$ and entropy $S = \ln(p/\rho^\gamma)$ of the mean flow and denoted by the tilde values

$$\begin{cases} \tilde{u} = \varepsilon\tau e^{\alpha(1-\tau^2)}\sin\theta \\ \tilde{v} = -\varepsilon\tau e^{\alpha(1-\tau^2)}\cos\theta \\ \tilde{T} = -\frac{(\gamma-1)\varepsilon^2 e^{2\alpha(1-\tau^2)}}{4\alpha\gamma} \\ \tilde{S} = 0, \end{cases} \tag{46}$$

where $\tau = r/r_c$ and $r = \sqrt{(x-x_c)^2 + (y-y_c)^2}$, $\varepsilon = 0.3$ indicates the strength of the vortex, $\alpha = 0.204$ controls the decay rate of the vortex and $r_c = 0.05$ is the critical radius for which the vortex has the maximum strength [3,29]. Fig. 8 shows the comparison of the pressure between different 7th-order WENO schemes along the center line of $y = 0.5$ at $t = 0.6$. The results are computed with the coarse mesh of 200×100, and the result obtained by 7th-order WENO-Z scheme with a refined mesh of 2000×1000 is given as the reference solution. It can be seen that the WENO-ZN scheme is more accurate than other WENO schemes.

4.4.3. Forward-facing step

The forward-facing step problem is also originally from the paper of [30]. The configuration of the problem is as follows: the two-dimensional wind tunnel spans a domain of $[0, 3] \times [0, 1]$, and a forward-facing step is located at $(0.6, 0.2)$. The problem is initialized by a right-going Mach 3 flow with a density of 1.4 and a pressure of 1. Reflective boundary conditions are applied along the walls of the tunnel, while inflow and outflow boundary conditions are set for the left and right boundaries, respectively. The density contours obtained by 7th-order WENO schemes with the mesh of 600×200 at $t = 4$ are shown

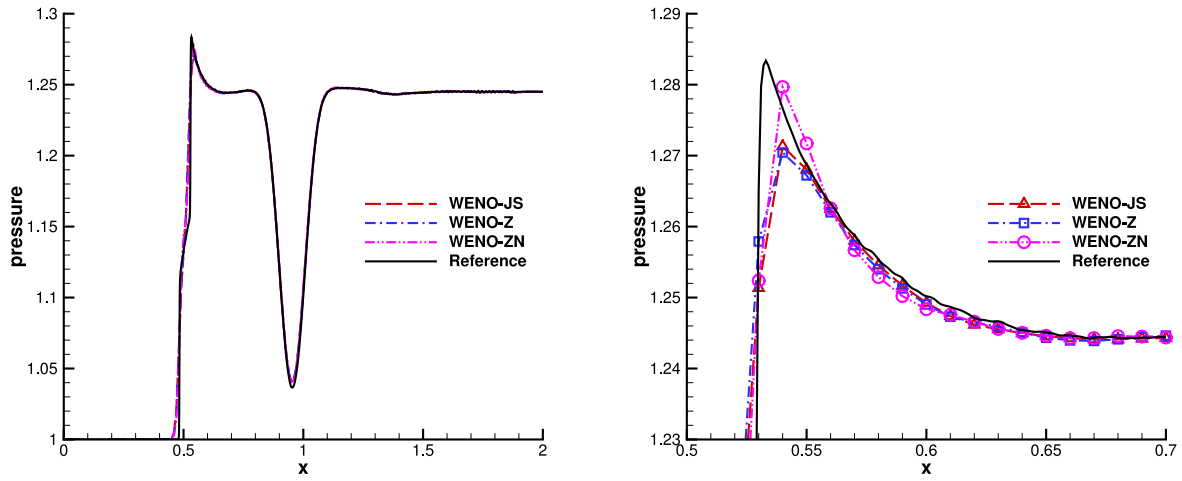

(a) Pressure distributions along the center line of $y = 0.5$

(b) Zoom-in view

Fig. 8. Numerical results of the shock/vortex interaction problem computed by the 7th-order WENO schemes with the mesh of 200 × 100 at $t = 0.6$.

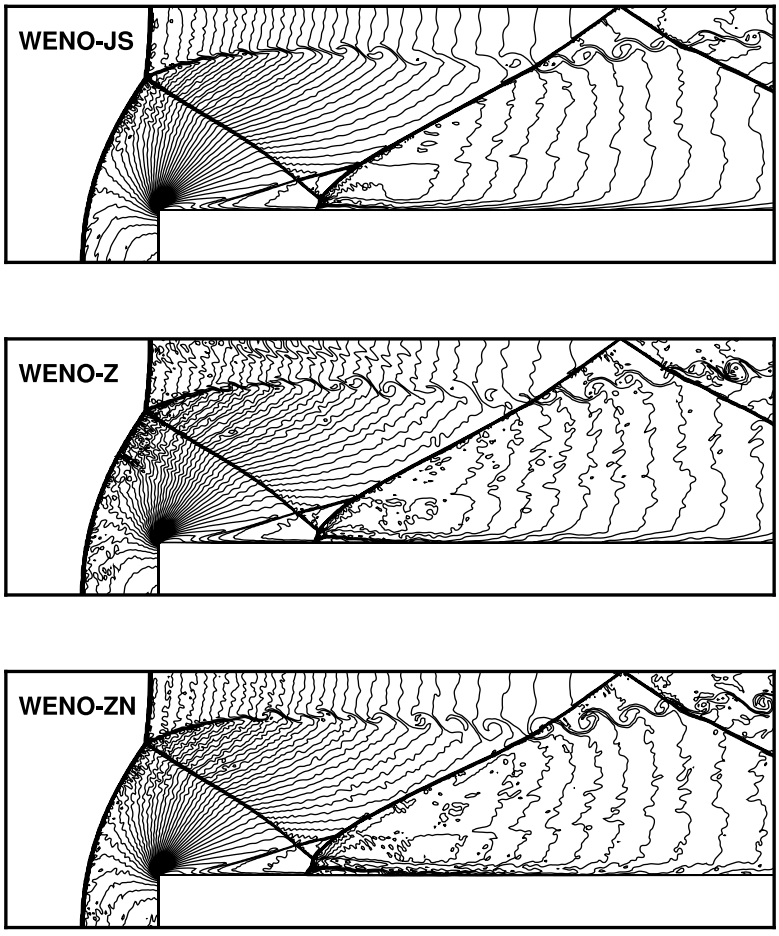

Fig. 9. Density contours of the forward-facing step problem computed by the 7th-order WENO schemes with the mesh of 600 × 200 at $t = 4$.

in Fig. 9. Numerical results show that all the schemes perform well with capturing shock waves, while the WENO-ZN scheme gives more clear roll-up structures of the vortex sheet caused by Kelvin–Helmholtz instability.

4.5. The evolution of taylor–Green vortex

The last example is the evolution of the three-dimensional inviscid Taylor–Green vortex [31–34]. Three-dimensional Euler equations are

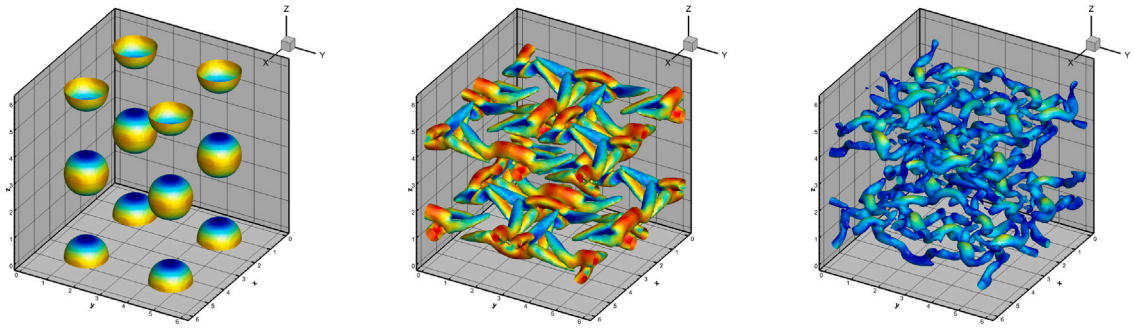

(a) $t = 0.0$, $\Omega = 1.5$ (b) $t = 4.978$, $\Omega = 3.0$ (c) $t = 10.0005$, $\Omega = 3.0$

Fig. 10. Isosurface of vorticity magnitude. The contour is given by velocity from 0 to 1.

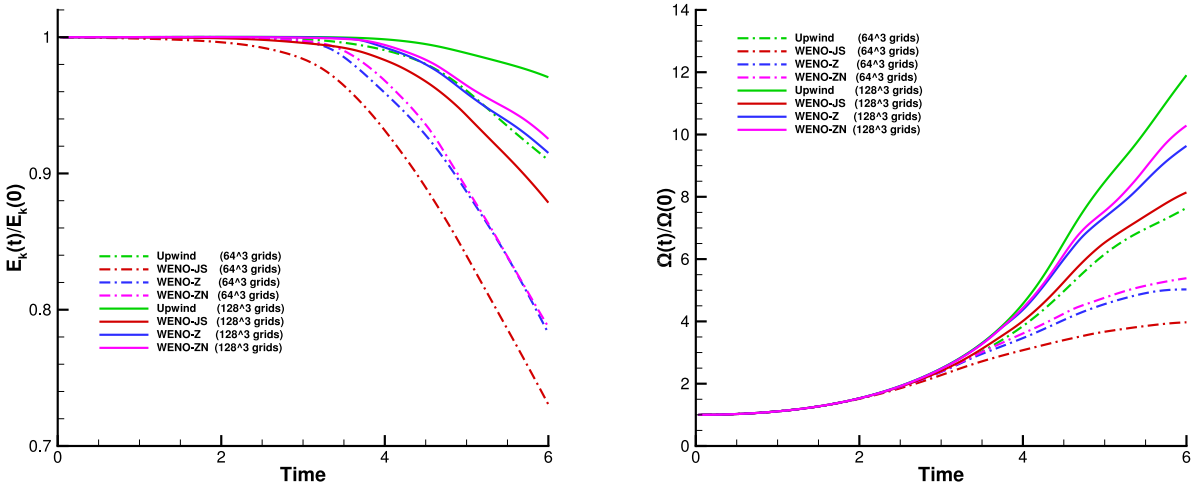

(a) kinetic energy (b) enstrophy

Fig. 11. Time-evolution of the normalized kinetic energy and the normalized enstrophy.

solved with $\gamma = 5/3$. The computational domain is $x_i \in [0, 2\pi)$ with periodic boundary conditions, and the initial conditions are

$$\begin{cases} \rho = 1 \\ u = \sin x \cos y \cos z \\ v = -\cos x \sin y \cos z \\ w = 0 \\ p = 100 + \frac{[\cos(2z)+2][\cos(2x)+\cos(2y)]-2}{16}. \end{cases} \tag{47}$$

Fig. 10 displays the evolution of the Taylor–Green vortex simulated by the seventh-order WENO-ZN scheme. Fig. 11 shows the temporal evolution of the mean kinetic energy $E_k(t)$ and enstrophy $\Omega(t)$ computed by the 7th-order upstream scheme, the WENO-JS scheme, the WENO-Z scheme and the WENO-ZN scheme with grids of 64^3 and 128^3.

$$E_k(t) = \frac{1}{L^3}\int_0^{2\pi}\int_0^{2\pi}\int_0^{2\pi} \rho\frac{\boldsymbol{u}(t)\boldsymbol{u}(t)}{2} dx dy dz. \tag{48}$$

$$\Omega(t) = \frac{1}{L^3}\int_0^{2\pi}\int_0^{2\pi}\int_0^{2\pi} \frac{\boldsymbol{\omega}(t)\boldsymbol{\omega}(t)}{2} dx dy dz. \tag{49}$$

In Fig. 11, the kinetic energy and enstrophy are normalized by their initial values.

As stated in [33], the evolution of inviscid Taylor–Green vortex flow in a three-dimensional periodic domain is perhaps the simplest model for investigation of the nonlinear transfer of kinetic energy among eddies with a range of spatial scales. For the Taylor–Green vortex flow, the normalized kinetic energy should maintain a constant value of nearly unity and the normalized enstrophy increases from unity to infinity by a finite time, as there is no dissipative mechanism in the system of partial differential equation. Hence, the evolution of Taylor–Green vortex flow provides a quantitative diagnostic of the intrinsic numerical dissipation and flow symmetry preservation in a discretization scheme for the Euler equation.

From Fig. 11 it can be seen that, the WENO-JS scheme dissipates the energy the most, and its dissipation on the refined meshes (128^3) is even larger than that of the seventh-order upwind scheme on the coarse meshes (64^3). The WENO-ZN scheme is less dissipative than both the WENO-JS and WENO-Z schemes. The numerical dissipation also reduces the sharpness of the approximation of derivatives, which results in the different growth rate of the enstrophy. It should be noted that, although the numerical kinetic energy dissipation of WENO-JS with meshes of 128^3 is larger than the one of the upwind scheme with meshes of 64^3, the enstrophy growth of the former is still faster than the latter. In all, the WENO-ZN scheme has the least numerical dissipation among the three WENO schemes.

5. Conclusion

The fifth-order WENO-ZN scheme is extended to higher-order schemes to improve the accuracy at high-order critical points. The high-order WENO-ZN schemes are more efficient for improving the accuracy at critical points than the high-order WENO-Zη schemes [20]. In addition, the WENO-ZN schemes can keep the ENO property very well, while the WENO-Zη schemes produce apparent oscillations for the shock tube problems. The new scheme is robust for capturing discontinuities and meanwhile has low dissipation and high resolution for refined structures.

CRediT authorship contribution statement

Shiyao Li: Conceptualization, Methodology, Software, Writing – original draft. **Yiqing Shen:** Funding acquisition, Supervision, Validation, Writing – review & editing. **Ke Zhang:** Software, Validation, Visualization. **Ming Yu:** Formal analysis, Validation, Visualization.

Declaration of competing interest

The authors declare that they have no known competing financial interests or personal relationships that could have appeared to influence the work reported in this paper.

Acknowledgment

This research work was supported by the National Natural Science Foundation of China under Grants 11872067, 91852203, 11902326, and 12172364.

References

[1] Harten A, Engquist B, Osher S, Chakravarthy SR. Uniformly high order accurate essentially non-oscillatory schemes, III. J Comput Phys 1987;71(2):231–303.
[2] Liu X-D, Osher S, Chan T. Weighted essentially non-oscillatory schemes. J Comput Phys 1994;115(1):200–12.
[3] Jiang G-S, Shu C-W. Efficient implementation of weighted ENO schemes. J Comput Phys 1996;126(1):202–28.
[4] Henrick AK, Aslam TD, Powers JM. Mapped weighted essentially non-oscillatory schemes: Achieving optimal order near critical points. J Comput Phys 2005;207(2):542–67.
[5] Borges R, Carmona M, Costa B, Don WS. An improved weighted essentially non-oscillatory scheme for hyperbolic conservation laws. J Comput Phys 2008;227(6):3191–211.
[6] Hu XY, Wang Q, Adams NA. An adaptive central-upwind weighted essentially non-oscillatory scheme. J Comput Phys 2010;229(23):8952–65.
[7] Ha Y, Ho Kim C, Ju Lee Y, Yoon J. An improved weighted essentially non-oscillatory scheme with a new smoothness indicator. J Comput Phys 2013;232(1):68–86.
[8] Fan P, Shen Y, Tian B, Yang C. A new smoothness indicator for improving the weighted essentially non-oscillatory scheme. J Comput Phys 2014;269:329–54.
[9] Acker F, Borges RB, Costa B. An improved WENO-Z scheme. J Comput Phys 2016;313:726–53.
[10] Liu S, Shen Y, Zeng F, Yu M. A new weighting method for improving the WENO-Z scheme. Internat J Numer Methods Fluids 2018;87(6):271–91.
[11] Baeza A, Bürger R, Mulet P, Zorío D. WENO Reconstructions of unconditionally optimal high order. SIAM J Numer Anal 2019;57(6):2760–84.
[12] Baeza A, Bürger R, Mulet P, Zorío D. An efficient third-order WENO scheme with unconditionally optimal accuracy. SIAM J Sci Comput 2020;42(2):A1028–51.
[13] Shen Y, Zhang K, Li S, Peng J. A novel method for constructing high accurate and robust WENO-Z type scheme. 2020, arXiv:2004.07954.
[14] Balsara DS, Shu CW. Monotonicity preserving weighted essentially non-oscillatory schemes with increasingly high order of accuracy. J Comput Phys 2000;160(2):405–52.
[15] Gerolymos G, Sénéchal D, Vallet I. Very-high-order weno schemes. J Comput Phys 2009;228(23):8481–524.
[16] Balsara DS, Rumpf T, Dumbser M, Munz C-D. Efficient, high accuracy ADER-WENO schemes for hydrodynamics and divergence-free magnetohydrodynamics. J Comput Phys 2009;228(7):2480–516.
[17] Balsara DS, Meyer C, Dumbser M, Du H, Xu Z. Efficient implementation of ADER schemes for Euler and magnetohydrodynamical flows on structured meshes – speed comparisons with Runge–Kutta methods. J Comput Phys 2013;235:934–69.
[18] Shen Y, Zha G. Improved seventh-order WENO scheme. AIAA paper 2010-1451, 2010.
[19] Castro M, Costa B, Don WS. High order weighted essentially non-oscillatory WENO-Z schemes for hyperbolic conservation laws. J Comput Phys 2011;230(5):1766–92.
[20] Fan P. High order weighted essentially nonoscillatory WENO-η schemes for hyperbolic conservation laws. J Comput Phys 2014;269:355–85.
[21] Wang Y, Wang BS, Don WS. Generalized sensitivity parameter free fifth order WENO finite difference scheme with Z-type weights. J Sci Comput 2019;81(3):1329–58.
[22] Don WS, Borges R. Accuracy of the weighted essentially non-oscillatory conservative finite difference schemes. J Comput Phys 2013;250:347–72.
[23] Pirozzoli S. On the spectral properties of shock-capturing schemes. J Comput Phys 2006;219(2):489–97.
[24] Shu C-W, Osher S. Efficient implementation of essentially non-oscillatory shock-capturing schemes. J Comput Phys 1988;77(2):439–71.
[25] Yamaleev NK, Carpenter MH. Third-order energy stable WENO scheme. J Comput Phys 2009;228(8):3025–47.
[26] Shi J, Zhang Y-T, Shu C-W. Resolution of high order WENO schemes for complicated flow structures. J Comput Phys 2003;186(2):690–6.
[27] Young Y, Tufo H, Dubey A, Rosner R. On the miscible Rayleigh-Taylor instability: two and three dimensions. J Fluid Mech 2001;447:377–408.
[28] Xu Z, Shu C-W. Anti-diffusive flux corrections for high order finite difference WENO schemes. J Comput Phys 2005;205(2):458–85.
[29] Liu S, Shen Y, Chen B, Zeng F. Novel local smoothness indicators for improving the third-order WENO scheme. Internat J Numer Methods Fluids 2018;87(2):51–69.
[30] Woodward P, Colella P. The numerical simulation of two-dimensional fluid flow with strong shocks. J Comput Phys 1984;54(1):115–73.
[31] Taylor GI, Green AE. Mechanism of the production of small eddies from large ones. Proc R Soc Lond Ser A-Math Phys Sci 1937;158(895):499–521.
[32] Orsag SA. Small-scale structure of the Taylor-Green vortex. Physica A 1984;124(1–3):521.
[33] Shu C-W, Don W-S, Gottlieb D, Schilling O, Jameson L. Numerical convergence study of nearly incompressible, inviscid Taylor–Green vortex flow. J Sci Comput 2005;24(1):1–27.
[34] Johnsen E, Larsson J, Bhagatwala AV, Cabot WH, Moin P, Olson BJ, Rawat PS, Shankar SK, Sjögreen B, Yee H, Zhong X, Lele SK. Assessment of high-resolution methods for numerical simulations of compressible turbulence with shock waves. J Comput Phys 2010;229(4):1213–37.